Article:
Amores, M., Baker, P.J., Cussen, E.J. et al. (2018) Na1.5La1.5TeO6:Na+ conduction in a novel Na-rich double perovskite. Chemical Communications, 54 (72). pp. 10040-10043. ISSN: 1359-7345

https://doi.org/10.1039/c8cc03367f

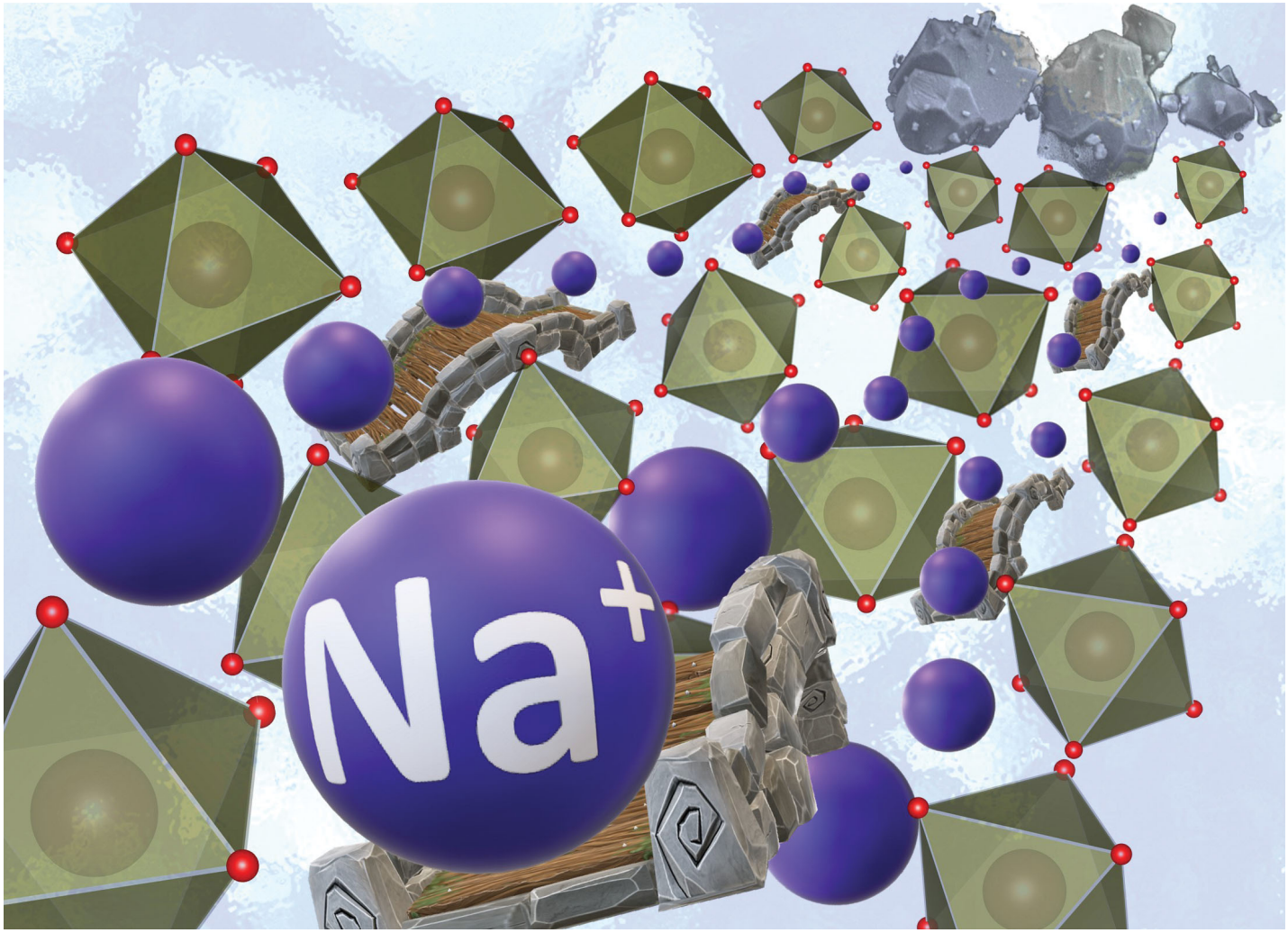

Showcasing collaborative research from Professor Serena Corr's laboratory, School of Chemistry, University of Glasgow and Dr Edmund Cussen, Department of Pure and Applied Chemistry, University of Strathclyde, Glasgow, United Kingdom.

$Na_{1.5}La_{1.5}TeO_6$: Na^+ conduction in a novel Na-rich double perovskite

Bridging of contiguous Na ions in the novel $Na_{1.5}La_{1.5}TeO_6$ Na-rich double perovskite ionic conductor material is enabled by the presence of Na ions in both A- and B-sites, resulting in a lower energy barrier for Na-ion diffusion.

As featured in:

See Serena A. Corr *et al.*, *Chem. Commun.*, 2018, **54**, 10040.

ROYAL SOCIETY OF CHEMISTRY

rsc.li/chemcomm

Registered charity number: 207890

ChemComm

COMMUNICATION

View Article Online
View Journal | View Issue

Cite this: *Chem. Commun.*, 2018, **54**, 10040

Received 25th April 2018,
Accepted 30th July 2018

DOI: 10.1039/c8cc03367f

rsc.li/chemcomm

$Na_{1.5}La_{1.5}TeO_6$: Na^+ conduction in a novel Na-rich double perovskite†

Marco Amores, [ab] Peter J. Baker, [c] Edmund J. Cussen [b] and Serena A. Corr *[a]

Increasing demand for lithium batteries for automotive applications, coupled with the necessity to move to large-scale energy storage systems, is driving a push towards new technologies and has seen Na-ion batteries emerge as a leading alternative to Li-ion. Amongst these, all solid-state configurations represent a promising route to achieving higher energy densities and increased safety. Remaining challenges include the need for Na^+ solid electrolytes with the requisite ionic conductivities crucial for use in a solid-state cell. Here, we present the novel Na-rich double perovskite, $Na_{1.5}La_{1.5}TeO_6$. The transport properties, explored at the macroscopic and local level, reveal a low activation energy barrier for Na^+ diffusion and great promise for use as an electrolyte for all solid-state Na-batteries.

The lower cost and greater availability of sodium compared to lithium, together with its similar redox couple potential of *ca.* 0.3 V lower for Na/Na^+ compared to Li/Li^+, has led to enormous interest in the development of Na batteries by the energy storage community over the last decade.[1] The larger cation size and heavier mass of sodium had made it a suitable candidate for medium to large-scale stationary energy storage applications, where gravimetric energy density is not a priority. As with Li-ion batteries, organic liquid Na-electrolytes present concerns in terms of safety and the operating voltage window available. The use of solid-state electrolytes in Na batteries could increase the energy density and safety of the battery, enable longer cyclability and permit the use of versatile cell geometries.[2,3] Current Na^+ solid-state electrolytes display Na^+ conductivities at room temperature from 10^{-10} S cm^{-1}, in the case of the $Na(B/Al)H_4$ complex hydrides, to benchmark values close to the mS cm^{-1} for the recently reported Na-containing chalcogenides.[2–4] Other systems include the NASICON phosphate materials, the classic β''-Al_2O_3 and the more recent layered P2-type $Na_2M_2TeO_6$ materials.[2,5] The electrolyte choice should fit the specific battery application, operating temperature and electrode in order to avoid malfunction. For example, β''-Al_2O_3 degrades with moisture content[6] and the room temperature superionic Na-containing sulfide materials suffer from poor electrochemical stability and reaction with Na metal electrodes.[7] Therefore, research on new Na^+ solid-state electrolyte systems that could meet requirements lacking in present systems is critical. Here, we present a new sodium-rich solid-state electrolyte $Na_{1.5}La_{1.5}TeO_6$, where the robust perovskite framework and redox stability of the Te^{6+} ions[8–12] could enable its use in combination with high voltage electrodes.

$A_2BB'O_6$ double perovskite structure allows for a wide range of potential compositions with multiple combinations of elements on the A, B and B′ sites, where B and B′ cation positions are ordered in the crystal structure.[13] The novel Na-rich $Na_{1.5}La_{1.5}TeO_6$ double perovskite presented here crystallises in the monoclinic $P2_1/n$ space group, with 1 mol of Na^+ and 1 mol of Te^{6+} cations occupying the octahedral B and B′ sites in a rock-salt type ordered fashion (Fig. 1). From the 2 mols of 8-fold coordinate A-sites, 1.5 mol is occupied by La^{3+} cations and 0.5 mols are occupied by additional Na^+, producing a ''Na-rich'' double perovskite with an expanded formula unit of $Na_{0.5}La_{1.5}NaTeO_6$. A similar alkali-metal rich double perovskite was reported by Rosseinsky and co-workers for the $Li_{1.5}La_{1.5}WO_6$ composition.[14] The discrepancy between the charges and sizes of the cations sitting in the A and BB′ sites produces the distortion of the symmetry from the ideal cubic structure to a monoclinic symmetry through an $a^-a^-b^+$ tilting system, as expected for a tolerance factor of 0.83 calculated for the $Na_{1.5}La_{1.5}TeO_6$ composition. The synthesis of $Na_{1.5}La_{1.5}TeO_6$ was achieved though an energy-efficient microwave-assisted solid-state synthesis. Such routes have been developed by our group in recent years for Li^+ solid electrolytes,[15–18] where the presence of hydroxide and oxide precursors increase the reaction kinetics by coupling effectively to microwave irradiation.[19]

[a] *School of Chemistry, University of Glasgow, Glasgow G12 8QQ, UK. E-mail: Serena.Corr@glasgow.ac.uk*
[b] *Department of Pure and Applied Chemistry, The University of Strathclyde, Thomas Graham Building, 295 Cathedral Street, Glasgow, G1 1XL, UK*
[c] *ISIS Pulsed Neutron and Muon Source, STFC Rutherford Appleton Laboratory, Harwell Science and Innovation Campus, Didcot, Oxfordshire OX11 0QX, UK*

† Electronic supplementary information (ESI) available. See DOI: 10.1039/c8cc03367f

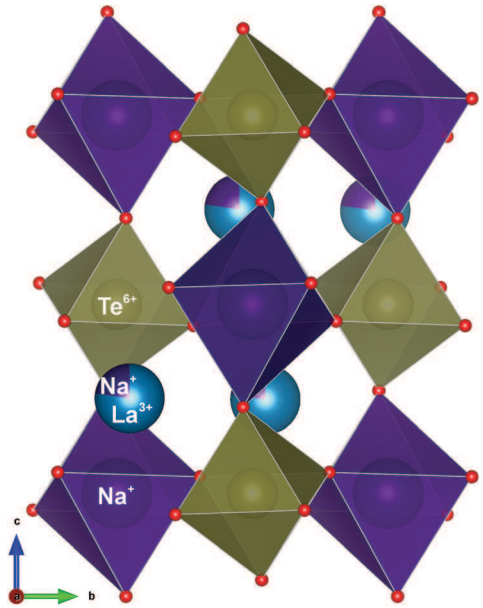

Fig. 1 Crystallographic representation of the $Na_{1.5}La_{1.5}TeO_6$ structure with monoclinic symmetry $P2_1/n$, where brown spheres represent octahedrally coordinated Te^{6+} ions, blue spheres represent 8-fold coordinated La^{3+} ions, purple spheres are the Na^+ ions and the oxygen anions are represented in red.

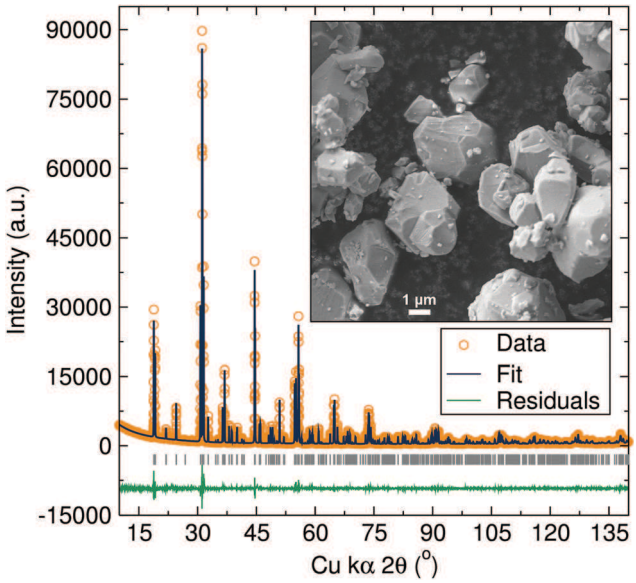

Fig. 2 Rietveld refinements of XRD data for the $Na_{1.5}La_{1.5}TeO_6$ double perovskite to the $P2_1/n$ monoclinic space group. Bragg peaks positions for the monoclinic $P2_1/n$ structure are indicated by vertical grey tick marks. Fit in excellent agreement to monoclinic space group $P2_1/n$, with cell parameters a = 5.69186(2) Å, b = 5.83933(2) Å, c = 8.13119(3) Å, β = 90.186(1)° and V = 270.253(1) Å^3. R_{wp} = 0.0743, R_{exp} = 0.0530 and χ^2 = 7.051. Inset: SEM image of $Na_{1.5}La_{1.5}TeO_6$ double perovskite.

The structure of the $Na_{1.5}La_{1.5}TeO_6$ double perovskite with monoclinic $P2_1/n$ symmetry was established by Rietveld refinements of powder XRD data (Fig. 2). As expected, Na^+ and Te^{6+} cations occupy the rock salt ordered B and B′ sites and refinement of site occupancies (Table S1, ESI†) indicated the presence of ~25% vacancies on the La^{3+} occupying the A-site, reminiscent of the related $Li_{1.5}La_{1.5}WO_6$ double perovskite.[14] Na^+ was refined into these vacant A-sites unoccupied by the La^{3+}, giving an A-site occupancy for this additional Na^+ of 0.239(2) which fills the available A-site vacancies. The calculated angle for the Na_B–O–Te was 152.1(4)°, resulting in a Glazer tilt of 13.9°, in good agreement with the related $Li_{1.5}La_{1.5}WO_6$ material (~13.6°).[14] The precision in the atomic parameters of Na^+ and O^{2-} is necessarily lower than for the stronger X-ray scatters La^{3+} and Te^{6+}, but the high atomic displacement parameters of the Na^+ ions may be indicative of mobility. The stoichiometry from Rietveld refinement was found to be $Na_{1.48(1)}La_{1.534(4)}TeO_6$, which was further confirmed by EDX analyses, where an atomic ratio of $Na_{1.52(8)}La_{1.48(4)}Te_{1.00(4)}$ was found (Fig. S2, ESI†), in excellent agreement with XRD and the target stoichiometry. Raman analysis (Fig. S1, ESI†) also confirmed the presence of vibrational bands corresponding to the monoclinic $P2_1/n$ group and the absence of carbonate or hydroxide moieties that could arise from secondary phases, typically invisible to laboratory XRD. The material microstructure was studied by SEM (Fig. 2 inset). The $Na_{1.5}La_{1.5}TeO_6$ particles had sizes ranging from 1 to 5 μm, with irregular, faceted morphologies.

To investigate the ionic macro- and microtransport properties of the $Na_{1.5}La_{1.5}TeO_6$ materials, electrochemical impedance spectroscopy and muon spin relaxation measurements (μ^+SR) were carried out. Fig. 3a shows the Nyquist plots of the impedance measurements, where two main components are observed. A semicircle component is noted at high frequencies, due to the resistance of the material towards ionic diffusion, and a second component in form of a linear tail can be seen at low frequencies resulting from the sodium-blocking gold electrodes employed in these measurements, indicating the predominantly ionic character of the observed impedance.[20] These data were fitted using equivalent electrical circuit composed of a resistor in parallel with a constant phase element, in series with a Warburg resistance. This gave a value for the ionic conductivity of $Na_{1.5}La_{1.5}TeO_6$ at room temperature of 5.4×10^{-8} S cm^{-1}. This is on the order of that first reported for phosphate NASICON materials, which has since seen improvements up to 10^{-3} S cm^{-1} through stoichiometric and structure-tailoring strategies.[21–25] These structure-tailoring strategies include element substitutions in the NASICON framework to increase the carrier concentrations or to increase the conduction channel size and hence the ionic conductivity of these materials.[26,27] In the case of the P2-type $Na_2M_2TeO_6$ tellurates oxides materials, the original work reported conductivities of 10^{-6} S cm^{-1} which have been now optimized to reach the mS cm^{-1} range.[5,12] It is reasonable to expect therefore that similar improvements are possible for the $Na_{1.5}La_{1.5}TeO_6$ double perovskite presented here through, for example, aliovalent doping or morphological control.

The activation energy required for macroscopic ionic conduction, calculated from an Arrhenius plot of EIS data, showed a promising value of 0.27(2) eV (Fig. 3c). This value is significantly lower compared to that obtained for the analogous

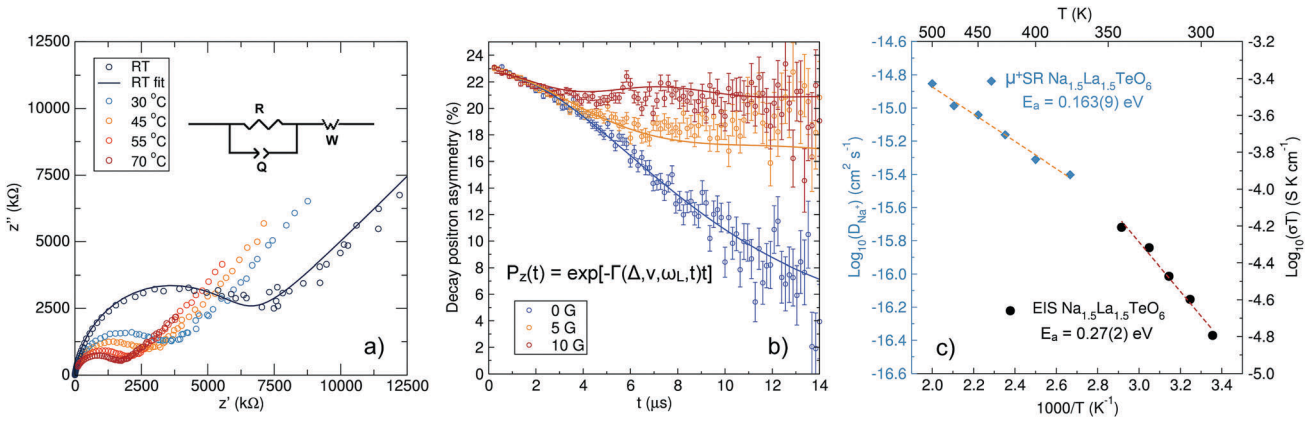

Fig. 3 (a) Nyquist plot of EIS data for $Na_{1.5}La_{1.5}TeO_6$ at different temperatures and a representative fit to the equivalent electrical circuit. (b) Room temperature μ^+SR data collected for $Na_{1.5}La_{1.5}TeO_6$ at zero field and applied longitudinal fields of 5 G and 10 G, fitted (solid lines) using the Keren function. (c) Arrhenius plots of the ionic conductivity and diffusion coefficient of $Na_{1.5}La_{1.5}TeO_6$ from μ^+SR and EIS.

$Li_{1.5}La_{1.5}WO_6$ double perovskite material of 0.50(5) eV.[14] This lower energetic requirement for ionic diffusion found for $Na_{1.5}La_{1.5}TeO_6$ could be related to the high relative density of the sintered material, nearly 96%, which results in a lower inter-grain energy requirement for Na^+ diffusion between sintered particles. The macroscopic activation energy found for this Na-rich double perovskite is similar to current benchmark systems with low activation energy values from EIS measurements,[2,3,28] for example Na_3PSe_4 which displays an activation energy of 0.21 eV.[29] Preliminary EIS analysis of a Na-metal electrode-sandwiched $Na_{1.5}La_{1.5}TeO_6$ cell at 80 °C revealed the lack of a Warburg element, confirming Na^+ as the conducting species (Fig. S3, ESI†). An increase in impedance over time is observed, which may point to a reaction with the sodium metal electrode at this temperature. Further examination of this, together with the use of similar protection approaches used for Li-metal anodes, could overcome these compatibility issues at high temperatures.[30,31]

The local Na^+ diffusion properties were also investigated by μ^+SR measurements performed on the EMU instrument at the ISIS Neutron and Muon source. The use of μ^+SR as a local probe to study Li^+ and Na^+ diffusion in battery materials has grown in recent years.[15,32–34] The natural abundance of the spin 1/2 ^{23}Na isotope is 100%, making Na^+ an ideal candidate to be studied by μ^+SR. The temporal evolution of the decay positron asymmetry for $Na_{1.5}La_{1.5}TeO_6$ at three different longitudinal magnetic fields is shown in Fig. 3b. At short times, the decay positron asymmetry followed a moderate decay, while at longer times the asymmetry decrease followed a slower trend, as expected for this Na-rich double perovskite with no paramagnetic ions in its structure and which also contains active nuclear spins (^{23}Na, ^{139}La and ^{125}Te) which can interact with the muon spin. To obtain the fluctuation rate of the muons due to sodium-ion diffusion (Fig. S4, ESI†), the muon decay asymmetry data were fitted using Keren's analytic generalization of the Abragam function (Fig. 3b).[35] The Na^+ diffusion coefficients from the muon fluctuation rate at different temperatures were then calculated applying eqn (1),[36] where N_i is the number of accessible Na sites in the i-th path, $Z_{v,i}$ is the vacancy fraction of the destination sites, s_i the jump distance between Na^+ sites, and ν the calculated muon fluctuation rate at each temperature.

$$D_{Na^+} = \sum_{i=1}^{n} \frac{1}{N_i} Z_{v,i} s_i^2 \nu \quad (1)$$

Since a detailed model of the Na^+ diffusion pathways for this novel Na-rich double perovskite is still not available, a simplified model based on the calculations reported by Rosseinsky and co-workers for the $Li_{1.5}La_{1.5}WO_6$ perovskite was employed.[14] The model is shown in Fig. S5 (ESI†) where Na^+ diffuses from the A sites to the two neighbouring B sites and from the B sites to the four neighbouring A sites, creating a 3D network for Na^+ diffusion. Additionally, a conservative 0.01 vacancy fraction in the Na^+ positions was introduced in both A and B sites to allow diffusion. From this preliminary model, and introducing the two different Na_A–Na_B distances of 3.33 and 3.46 Å, a Na^+ diffusion coefficient at room temperature of 4.2×10^{-12} cm^2 s^{-1} was obtained. This diffusion coefficient is similar to that reported for the $Na_x(Mn/Co)O_2$ layered cathode materials (10^{-11}–10^{-12} cm^2 s^{-1}), indicating excellent compatibility of these components in terms of Na^+ diffusion.[34,37,38] The microscopic diffusion of $Na_{1.5}La_{1.5}TeO_6$ is also in line with other Na^+ ionic conductors such as the $Na_xWO_2Cl_2$ tungsten bronze with a Na^+ diffusion coefficient of 10^{-13} cm^2 s^{-1},[39] and Na_3PS_4 with a value in the range of 10^{-12} cm^2 s^{-1}.[40] The μ^+SR measurements indicate that the activation energy required for local Na^+ diffusion is 0.163(9) eV. This low activation energy is similar to related oxide materials, such as the Ga-doped $Na_2Zn_2TeO_6$ with an activation energy of 0.12 eV as observed from NMR measurements,[12] or β′-alumina single crystals with activations energies in the 0.12–0.16 eV range.[41]

The higher activation energy values obtained from the macroscopic EIS measurements which probes long range Na^+ conduction through multiple intra-grain crystalline sites and grain boundaries, compared to microscopic μ^+SR measurements which are more sensitive to individual Na^+ hops within

the crystalline grain, could have its origin in the contribution to the resistance from grain boundaries to ionic conduction which is virtually invisible to μ^+SR. Lower conductivity values and higher energy barriers to diffusion could also result from the presence of La^{3+} ions in the A-sites, which could hinder long-range Na^+ conductivity. Nevertheless, the excellent microscopic Na^+ transport properties displayed by this novel $Na_{1.5}La_{1.5}TeO_6$ Na-rich double perovskite indicates that, upon further optimization, this material could be a promising candidate as a solid electrolyte for Na batteries.

In conclusion, we have demonstrated the synthesis of a novel Na-rich double perovskite, $Na_{1.5}La_{1.5}TeO_6$ through microwave methods, which crystallises with monoclinic $P2_1/n$ space group with Na^+ on both the A- and B-sites. The material displays a macroscopic ionic conductivity on the order of 10^{-8} S cm^{-1} at room temperature with a low activation energy of 0.27(2) eV. μ^+SR measurements reveal a microscopic diffusion coefficient for Na^+ at room temperature in the order of 10^{-12} cm^2 s^{-1} and a very low activation energy of 0.163(9) eV. These findings reveal the promising transport properties for this $Na_{1.5}La_{1.5}TeO_6$ material and further developments are forthcoming to optimize the macroscopic transport to its maximum microscopic potential.

The authors gratefully acknowledge technical support from Michael Beglan. The authors also thank the EPSRC for funding (EP/N001982/1), the STFC for beamtime allocation, the Universities of Glasgow and Strathclyde for support and the use of facilities, and the School of Chemistry at Glasgow for PhD studentship funding.

Conflicts of interest

There are no conflicts to declare.

References

1 J.-Y. Hwang, S.-T. Myung and Y.-K. Sun, *Chem. Soc. Rev.*, 2017, **46**, 3529–3614.
2 J.-J. Kim, K. Yoon, I. Park and K. Kang, *Small Methods*, 2017, **1**, 1700219.
3 H. Che, S. Chen, Y. Xie, H. Wang, K. Amine, X.-Z. Liao and Z.-F. Ma, *Energy Environ. Sci.*, 2017, **10**, 1075–1101.
4 K. B. Hueso, M. Armand and T. Rojo, *Energy Environ. Sci.*, 2013, **6**, 734–749.
5 M. A. Evstigneeva, V. B. Nalbandyan, A. A. Petrenko, B. S. Medvedev and A. A. Kataev, *Chem. Mater.*, 2011, **23**, 1174–1181.
6 F. G. Will, *J. Electrochem. Soc.*, 1976, **123**, 834–836.
7 Z. Yu, S.-L. Shang, Y. Gao, D. Wang, X. Li, Z.-K. Liu and D. Wang, *Nano Energy*, 2018, **47**, 325–330.
8 A. Gupta, C. B. Mullins and J. B. Goodenough, *J. Power Sources*, 2013, **243**, 817–821.
9 M. Sathiya, K. Ramesha, G. Rousse, D. Foix, D. Gonbeau, K. Guruprakash, A. S. Prakash, M. L. Doublet and J.-M. Tarascon, *Chem. Commun.*, 2013, **49**, 11376–11378.
10 Z. Yang, Y. Jiang, L. Deng, T. Wang, S. Chen and Y. Huang, *J. Power Sources*, 2017, **360**, 319–323.
11 E. A. Zvereva, V. B. Nalbandyan, M. A. Evstigneeva, H.-J. Koo, M.-H. Whangbo, A. V. Ushakov, B. S. Medvedev, L. I. Medvedeva, N. A. Gridina, G. E. Yalovega, A. V. Churikov, A. N. Vasiliev and B. Büchner, *J. Solid State Chem.*, 2015, **225**, 89–96.
12 Y. Li, Z. Deng, J. Peng, E. Chen, Y. Yu, X. Li, J. Luo, Y. Huang, J. Zhu, C. Fang, Q. Li, J. Han and Y. Huang, *Chem. – Eur. J.*, 2018, **24**, 1057–1061.
13 S. Vasala and M. Karppinen, *Prog. Solid State Chem.*, 2015, **43**, 1–36.
14 A. B. Santibanez-Mendieta, C. Didier, K. K. Inglis, A. J. Corkett, M. J. Pitcher, M. Zanella, J. F. Shin, L. M. Daniels, A. Rakhmatullin, M. Li, M. S. Dyer, J. B. Claridge, F. Blanc and M. J. Rosseinsky, *Chem. Mater.*, 2016, **28**, 7833–7851.
15 M. Amores, T. E. Ashton, P. J. Baker, E. J. Cussen and S. A. Corr, *J. Mater. Chem. A*, 2016, **4**, 1729–1736.
16 M. Amores, S. A. Corr and E. J. Cussen, *J. Electrochem. Soc.*, 2017, **164**, A6395–A6400.
17 H. El-Shinawi, E. J. Cussen and S. A. Corr, *Dalton Trans.*, 2017, **46**, 9415–9419.
18 H. El-Shinawi, G. W. Paterson, D. A. MacLaren, E. J. Cussen and S. A. Corr, *J. Mater. Chem. A*, 2017, **5**, 319–329.
19 H. J. Kitchen, S. R. Vallance, J. L. Kennedy, N. Tapia-Ruiz, L. Carassiti, A. Harrison, A. G. Whittaker, T. D. Drysdale, S. W. Kingman and D. H. Gregory, *Chem. Rev.*, 2014, **114**, 1170–1206.
20 J. T. S. Irvine, D. C. Sinclair and A. R. West, *Adv. Mater.*, 1990, **2**, 132–138.
21 F. E. Mouahid, M. Bettach, M. Zahir, P. Maldonado-Manso, S. Bruque, E. R. Losilla and M. A. G. Aranda, *J. Mater. Chem.*, 2000, **10**, 2748–2757.
22 N. Anantharamulu, K. Koteswara Rao, G. Rambabu, B. Vijaya Kumar, V. Radha and M. Vithal, *J. Mater. Sci.*, 2011, **46**, 2821–2837.
23 H. Park, K. Jung, M. Nezafati, C.-S. Kim and B. Kang, *ACS Appl. Mater. Interfaces*, 2016, **8**, 27814–27824.
24 S. Song, H. M. Duong, A. M. Korsunsky, N. Hu and L. Lu, *Sci. Rep.*, 2016, **6**, 32330.
25 P. Colomban, *Solid State Ionics*, 1986, **21**, 97–115.
26 K. Arbi, J. M. Rojo and J. Sanz, *J. Eur. Ceram. Soc.*, 2007, **27**, 4215–4218.
27 A. Martínez-Juárez, C. Pecharromán, J. E. Iglesias and J. M. Rojo, *J. Phys. Chem. B*, 1998, **102**, 372–375.
28 V. S. Kandagal, M. D. Bharadwaj and U. V. Waghmare, *J. Mater. Chem. A*, 2015, **3**, 12992–12999.
29 L. Zhang, K. Yang, J. Mi, L. Lu, L. Zhao, L. Wang, Y. Li and H. Zeng, *Adv. Energy Mater.*, 2015, **5**, 1501294.
30 X.-B. Cheng, R. Zhang, C.-Z. Zhao and Q. Zhang, *Chem. Rev.*, 2017, **117**, 10403–10473.
31 S. Wenzel, T. Leichtweiss, D. A. Weber, J. Sann, W. G. Zeier and J. Janek, *ACS Appl. Mater. Interfaces*, 2016, **8**, 28216–28224.
32 T. E. Ashton, J. V. Laveda, D. A. MacLaren, P. J. Baker, A. Porch, M. O. Jones and S. A. Corr, *J. Mater. Chem. A*, 2014, **2**, 6238–6245.
33 J. V. Laveda, B. Johnston, G. W. Paterson, P. J. Baker, M. G. Tucker, H. Y. Playford, K. M. Jensen, S. J. Billinge and S. A. Corr, *J. Mater. Chem. A*, 2018, **6**, 127–137.
34 M. Månsson and J. Sugiyama, *Phys. Scr.*, 2013, **88**, 068509.
35 A. Keren, *Phys. Rev. B: Condens. Matter Mater. Phys.*, 1994, **50**, 10039–10042.
36 *An Introduction to Solid State Diffusion*, ed. R. J. Borg, G. Dienes, Academic Press, San Diego, 1988.
37 A. Mendiboure, C. Delmas and P. Hagenmuller, *J. Solid State Chem.*, 1985, **57**, 323–331.
38 A. Bhide and K. Hariharan, *Solid State Ionics*, 2011, **192**, 360–363.
39 P. G. Bruce, J. Nowinski and V. C. Gibson, *Solid State Ionics*, 1992, **50**, 41–45.
40 Z. Zhu, I.-H. Chu, Z. Deng and S. P. Ong, *Chem. Mater.*, 2015, **27**, 8318–8325.
41 Z. Yang, J. Zhang, M. C. W. Kintner-Meyer, X. Lu, D. Choi, J. P. Lemmon and J. Liu, *Chem. Rev.*, 2011, **111**, 3577–3613.